Trimeric Chromium Oxyformate Route to Chromia-Pillared Clay

Joo-Byoung Yoon, Sung-Ho Hwang, and Jin-Ho Choy*

National Nanohybrid Materials Laboratory, School of Chemistry & Molecular Engineering, Seoul National University, Seoul 151-747, Korea
Received August 7, 2000

A chromia-pillared clay has been prepared by ion exchange type intercalation reaction between the sodium ion in montmorillonite and the trimeric chromium oxyformate (TCF) ion, and by subsequent heat-treatment. The structural and thermal properties have been systematically studied by thermal analysis, powder XRD, IR spectroscopy, and XAS. The gallery height of ~6.8 Å upon intercalation of the TCF ion suggests that the Cr_3O plane is parallel to the aluminosilicate layers. Even though the basal spacing of TCF intercalated clay decreases slightly upon heating, the layer structure was retained up to 550 °C as confirmed by XRD and TG/DTA. According to the EXAFS spectroscopic analysis, it is identified that the (Cr-Cr) distance of 3.28 Å between vertex-linked CrO_6 octahedra in TCF splits into 2.64 Å, 2.98 Å, and 3.77 Å due to the face-, edge-, and corner-shared CrO_6 octahedra after heating at 400 °C, implying that a nano-sized chromium oxide phase was stabilized within the interlayer space of clay.

Introduction

There has been considerable interest in introducing small robust particles of metal oxides or chalcogenides into the interlamella region of swelling clays in order to keep the layers apart, thus resulting in internal surfaces available for adsorption or catalysis.[1-4] To prepare an expanded clay with a high porosity various organic molecules have been used as intercalants,[5] but it was proved to be not sustainable in the temperature range 250-500 °C. And thereafter, attempts have been made to realize a thermally stable pillared clay by using aluminum hydroxides and other various inorganic oxides or oxide sols as intercalants.[6-8] Clays intercalated by certain polyoxocations are of particular importance, because they can be converted to porous pillared clays containing molecular-sized oxides upon dehydration and dehydroxylation.[9] The type of poly-nuclear metal species immobilized in the interlayers determines the characteristics of pillared materials such as surface area, porosity, acidity and catalytic activity.

Among many metal species, chromium oxide is a very well-known catalyst for the selective dehydrogenation of cyclohexane.[9] It has also been reported that μ-oxotrinuclear mixed valent and mixed metal carboxylate complexes with chromium ions have been used in the catalytic oxidation of styrene and cumene where the main products were styrene oxide and benzaldehyde.[10] Therefore, much effort has been paid to obtain highly porous pillared clays with various polycations of Cr^{3+}.[9,11,12] In order to understand such catalytic activities, it is necessary to solve the crystal structure of pillared clay, especially, nano-sized inorganic oxide pillars. In general, it has been proven to be very difficult to characterize the polynuclear metal oxide pillar in the clay, though many attempts have been made by using magic angle spinning nuclear magnetic resonance (MAS-NMR) spectroscopy as demonstrated for Al-based pillars.[13] However, for other transition metal oxide pillars such as chromia one, this technique is not applicable. Moreover, the precise chemical species beyond oligomeric hydroxy aquo-units and the reaction mechanism during ion exchange reaction and calcination remain unclear up to now.

For this reason, the application of extended X-ray absorption fine structure (EXAFS) and X-ray absorption near edge structure (XANES) spectroscopies in determining the electronic and geometric structures of a pillar in layered matrix is very useful. These techniques are quite appropriate in observing the local environment of interlayer cations due to their sensitivity to a specific atom and its local order. And moreover the absorption coefficient of main elements in the silicate matrix is fairly low, which could provide a sensitivity to the intercalated polynuclear metal species even with a minor concentration.[14] In this regard, we have recently carried out structural studies on the copper complex intercalated layer silicates,[15] the organic alkoxide substituted FeOCl,[16] and SiO_2-TiO_2-pillared clay[17] *via* EXAFS technique.

As an extension of the above works, we attempted to intercalate trimeric chromium oxyformate (TCF) ions, $[Cr_3O(HCO_2)_6(H_2O)_3]^+$, into the interlayer space of clay in order to keep the mineral layers apart, and to prepare the chromia pillared clay with high thermal stability by subsequent heating. We made use of powder X-ray diffraction (XRD), Cr K-edge X-ray absorption spectroscopy (XAS) and other optical spectroscopies such as infra-red spectroscopy (IR) and diffuse reflectance spectroscopy (DRS) to prove the structural details and the oxidation state of chromium species upon the pillaring reaction.

Experimental Section

TCF was prepared as described in the literature.[18] The chromic hydroxide freshly precipitated from chromic chloride (8 g) was dissolved in formic acid (8 mL), and the reac-

*To whom all correspondence should be addressed. Tel: +82-2-880-6658, Fax: +82-2-872-9864, E-mail: jhchoy@plaza.snu.ac.kr

tion product was crystallized upon slow cooling.

For ion exchanging type intercalation reaction, montmorillonite (Bentonite from Junsei Chem.) was converted into a sodium form by treating it with 1 N NaCl solution, and the excess salt was then removed by washing with distilled water for several times. This sodium-saturated sample was then fractionated by Stokes' law with a particle size below 2 μm. The montmorillonite-TCF complex was prepared by mixing the Na-montmorillonite suspension with aqueous trimeric chromium oxyformate chloride (TCF-Cl) solution and reacting at 65 °C for 48 hours. The ion-exchanged clay was centrifuged and washed with deionized water to remove excess salt until the clay suspension gave colorless supernatant and the $AgNO_3$ test showed a negative response. The product was dried at 80 °C (TCF-IM), and then calcined at 250 °C (TCF-PILC250) and 400 °C (TCF-PILC400) under an ambient atmosphere.

XRD measurements were performed by a JEOL JDX diffractometer with Ni-filtered Cu-K$_\alpha$ radiation (λ = 1.5418 Å). Diffuse reflectance UV-Visible spectra were recorded at room temperature on a Perkin Elmer UV/VIS Lambda 12 spectrophotometer. $BaSO_4$ was used as a reference material. The elemental analyses for C, H, and N were performed by CHN analyzer (Carlo Erba 1108) and the contents of metal species were determined by inductively coupled plasma. TG/DTA was measured by a Rigaku TAS100 thermal analyzer (RT~600 °C, ambient atmosphere, heating rate 10 °C/min). IR and BET surface area were measured by a Perkin-Elmer 1710 FT-IR (400-4000 cm^{-1}) and by a Micrometrics Autosorb 2100E, respectively. Electron paramagnetic resonance spectra were also recorded by an E-3 Varian X-band spectrometer at room temperature. The g values were calculated relative to a 2,2'-diphenyl-1-picrylhydrazyl (DPPH) standard.

XAS measurements were carried out with synchrotron radiation using the EXAFS facility installed at the beam line 7C in Photon Factory, High Energy Accelerator Research Organization (KEK), operated at 2.5 GeV with *ca.* 260-370 mA of stored current.[19] A Si(111) double-crystal monochromator was employed and higher order harmonics were rejected by detuning 30% from the maximum incident intensity. All the data were recorded in a transmission mode at room temperature using N_2- and (25% Ar + 75% N_2)-filled ionization chambers for I_0 and I_t, respectively.

The data analyses for experimental spectra were performed by the standard procedure as previously described.[20,21] The photon energies of all XANES spectra were calibrated by the first absorption peak of a chromium metal foil spectrum, located at 5989 eV. The inherent background was removed from all spectra by polynomial fitting of the pre-edge region and subtracting this fitted background from the entire spectrum. The resulting spectra were normalized by adjusting an edge jump to unity. For the EXAFS analysis, the absorption spectrum for the isolated atom, $\mu_0(E)$, was approximated by some cubic splines ($\mu(E)$). The EXAFS function, $\chi(E)$, was obtained as $\chi(E) = \{\mu(E) - \mu_0(E)\}/\mu_0(E)$. The resulting EXAFS spectra were k^3-weighted in order to compensate for the attenuation of EXAFS amplitude at high k, and then Fourier transformed in the range ~2.5 Å^{-1} $\leq k \leq$ ~13.5 Å^{-1} with a Hanning apodization function.

In order to determine the structural parameters, a nonlinear least-squares curve fitting was performed in the R-space of the Fourier transform (FT), using UWXAFS2 code.[22] The backscattering amplitude, $F_i(k)$, the total phase shift, $\phi_i(k)$, and the photoelectron mean free path, $\lambda(k)$, have been theoretically calculated for all scattering paths including multiple scattering by a curved wave *ab initio* FEFF 6.[23,24] In the course of nonlinear least-squares curve fitting, coordination number (N_i), bond distance (R_i), Debye-Waller factor (σ_i^2), and threshold energy difference (ΔE_0) were optimized as variables.

Results and Discussion

Structural description for the TCF ion. The complex TCF ion has 3/*m* point group symmetry, in which the chromium atoms are at the apices of an equilateral triangle with an edge distance of 3.28 Å. The three chromium octahedra are shared by a common vertex, where a single oxygen (O_{ap}) atom occupies this shared vertex. Three transpositions of this apical oxygen are occupied by three water molecules (H_2O). The four remaining positions of each chromium octahedron are occupied by four oxygen atoms from different formate groups ($O_{formate}$). Thus the formate groups form bridges between adjacent atoms on vertices as illustrated in Figure 1. Thus the Cr-O distances are ranging from 1.9 Å to 2.1 Å with a mean value of 2.0 Å similar to that of an acetato-complex.[25]

Powder XRD and TG/DTA of TCF-montmorillonite. Powder XRD analyses were carried out for the TCF-IM and its calcined derivatives prepared at 250 °C and 400 °C, respectively as shown in Figure 2. The basal spacing of 16.4 Å upon intercalation of the TCF ion suggests that the Cr_3O plane is parallel to the sheets of aluminosilicates. Even though the basal spacing decreases slightly from 16.4 Å to 15.8 Å upon heating at 400 °C, the two-dimensional structure remains unchanged at least up to 550 °C as confirmed by the well-developed (00*l*) reflections. Such a result indicates that the pillaring reaction proceeds topotatically. After calcining at 400 °C, it transforms into microporous Cr_2O_3-pillared montmorillonite with a specific surface area of 152

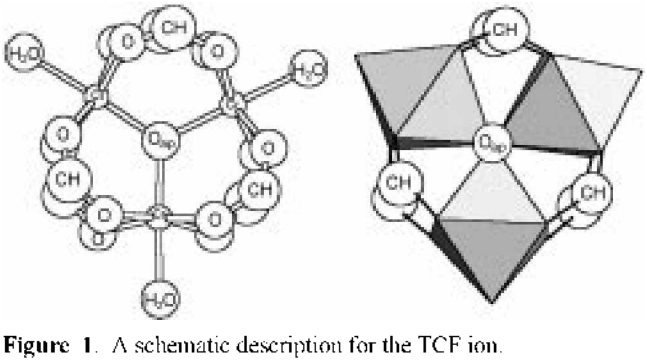

Figure 1. A schematic description for the TCF ion.

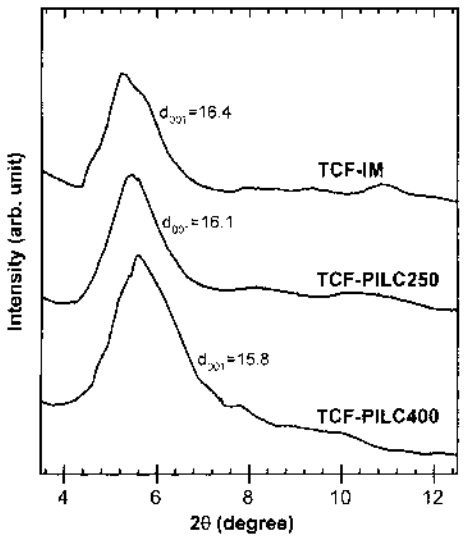

Figure 2. Powder XRD patterns for TCF-pillared clay. (a) TCF-IM, (b) TCF-PILC250, and (c) PILC400.

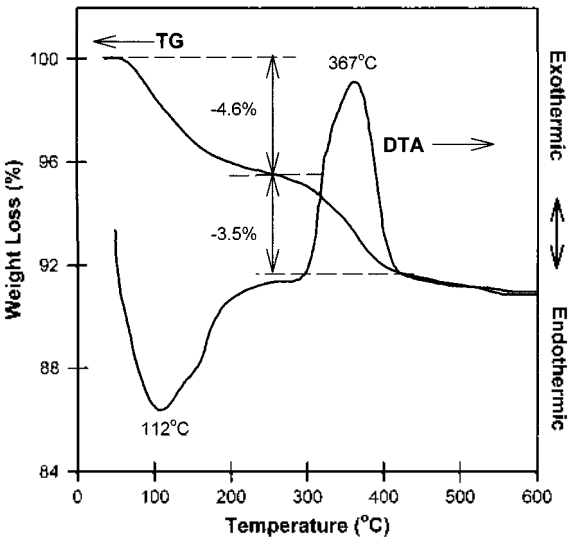

Figure 3. TG/DTA results for TCF-pillared clay.

m^2/g.

In order to investigate the thermal behavior of chromia-pillared clay, TG/DTA measurement was carried out under an ambient atmosphere (Figure 3). Two distinct weight losses in the TG curve are found at around 112 °C and 367 °C, respectively. The first endothermic peak is due to the loss of free water in the interlayer space and the second exothermic one can be assigned to the decomposition of organic moieties of the intercalated TCF ion. No distinct thermal event can be observed beyond 400 °C, implying that the pillaring process was already completed, and powder XRD confirmed that the pillared clay was thermally stable up to 550 °C.

IR spectra. IR spectra for TCF-Cl, TCF-IM and TCF-PILCs in the range of 400-2000 cm^{-1} are shown in Figure 4. The IR spectrum of TCF-Cl itself exhibits the characteristic bands of a bidentate COO^- group and the Cr_3O plane. The

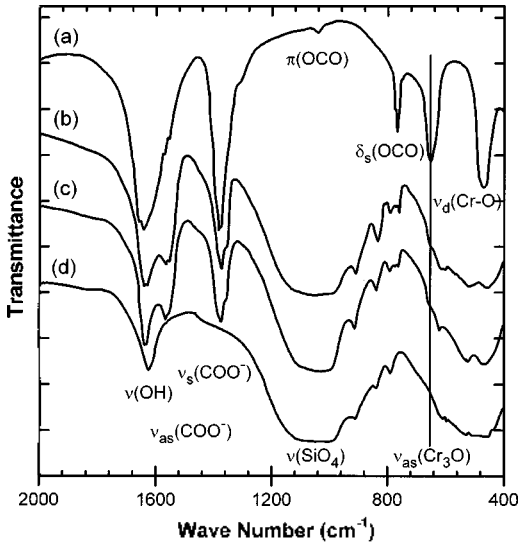

Figure 4. IR spectra for (a) TCF-Cl, (b) TCF-IM, (c) TCF-PILC250, and (d) PILC400.

symmetric and asymmetric stretching vibrations of COO^- are observed at 1573 cm^{-1} as a shoulder and 1380 cm^{-1} as a strong peak, respectively, together with a strong 1650 cm^{-1} peak due to the ν(O-H) of water. Some weak bending modes are also observed at 1044 cm^{-1} due to π(OCO) and 770 cm^{-1} due to δ_s(OCO). A strong asymmetric stretching ν_{as} due to (Cr_3O) is observed at 655 cm^{-1}, and a strong ν_d(Cr-O) vibration due to 3-planar D_{4h} units interacting under D_{3h} symmetry also appears at 468 cm^{-1}.[26]

According to the IR spectra of TCF-IM and heat-treated TCF-PILC 250, the bands at around 660 cm^{-1}, 1570 cm^{-1} and 1380 cm^{-1} are appeared, due to the TCF ion, together with the broad peaks due to montmorillonite. However, at 400 °C, the bands due to the TCF ion disappear completely. Although some peaks are ambiguous because of the overlap with those of the layered silicate, these facts unquestionably indicate that the CrO_3 unit of the TCF ion remains at least up to 250 °C and then decomposes beyond 400 °C as expected from the thermal analysis.

EPR and diffuse reflectance spectra. EPR spectra for TCF-IM and TCF-PILCs exhibited a broad, isotropic band centered on $g = 1.98$ with a width of several hundred gauss, which is the characteristic signal of octahedrally coordinated Cr^{3+}.[27] The splitting was not observed, indicating that there are no other valence states in the samples.

Figure 5 shows the relative DRS absorbance for the chromium-containing clays depending on calcination temperature. For TCF-IM, two broad absorption bands are observed around ~380 nm and ~505 nm, those which are the characteristic value of Cr^{3+} ions in an octahedral symmetry as reported in chromium acetates.[28] These peaks are assigned as $^4A_{2g} \rightarrow {}^4T_{1g}$ (ν_2) and $^4A_{2g} \rightarrow {}^4T_{2g}$ (ν_1) transitions and red-shifted to ~420 nm and ~565 nm as the calcination temperature increases. The values of crystal field parameters (Dq) and Racah inter-electronic repulsion parameters (B) are evaluated from the observed band energies using the following expressions:[29]

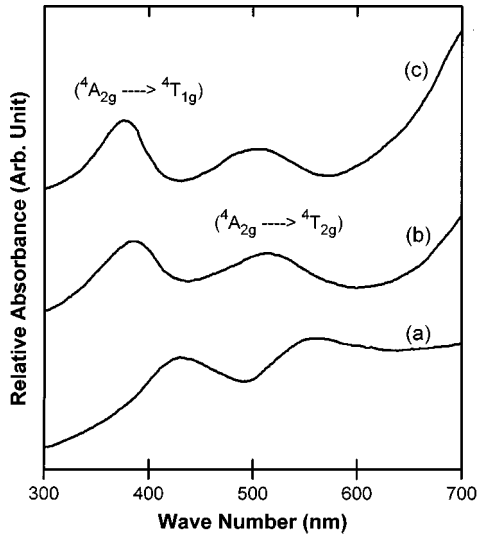

Figure 5. Diffuse reflectance spectra for (a) TCF-IM, (b) TCF-PILC250, and (c) PILC400.

$$Dq = \nu_1/10$$
$$B = (2\,\nu_1^2 + \nu_2^2 - 3\,\nu_1\,\nu_2) / (15\,\nu_2 - 27\,\nu_1).$$

where ν_1 and ν_2 correspond to the transition energy of $^4A_{2g} \rightarrow {}^4T_{2g}$ and $^4A_{2g} \rightarrow {}^4T_{1g}$, respectively.

The Racah and ligand field parameters (B and Dq) for TCF-IM are 667 cm^{-1} and 1942 cm^{-1}, and those for TCF-PILC400 are 505 cm^{-1} and 1786 cm^{-1}, respectively. The Racah parameter (B) for the free Cr^{3+} ion is 918 cm^{-1}, and therefore, the present B value strongly suggests that the bonding character is predominantly covalent, especially, for the calcined complex at 400 °C.[30,31]

XAS study for TCF-montmorillonite. In order to examine the evolution of electronic and geometric structures around Cr atom in TCF-IM and TCF-PILC400, XAS measurements were carried out at the Cr K-edge. In the Cr K-edge XANES spectra for the compounds (Figure 6), the edge energies and pre-edge intensities are quite similar indicating that the oxidation state of Cr^{3+} remains unchanged before and after calcination. Considering the weak pre-edge peaks (P) and their energy positions, no evidence could be found on the presence of Cr^{4+}, which was, however, previously observed in the hydrous chromium-pillared clays and the supported chromium catalysts.[32,33] On the other hand, we could observe a significant peak shift at around 6020 eV, which reflects the multiple scattering originated mainly from the first and second neighbors.[34] For the TCF-PILC400, the peak shifts to a higher energy side by ~10 eV compared to TCF-IM. Such a result represents the shortened distance between Cr and neighbors upon heating due to an enhancement of bond covalency.

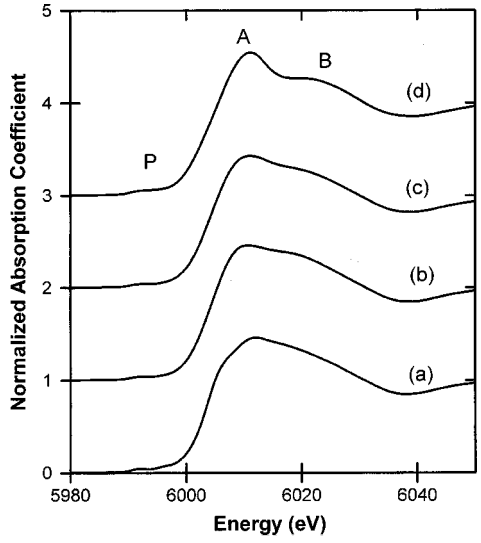

Figure 6. XANES spectra for (a) TCF-Cl, (b) TCF-IM, (c) TCF-PILC250, and (d) TCF-PILC400.

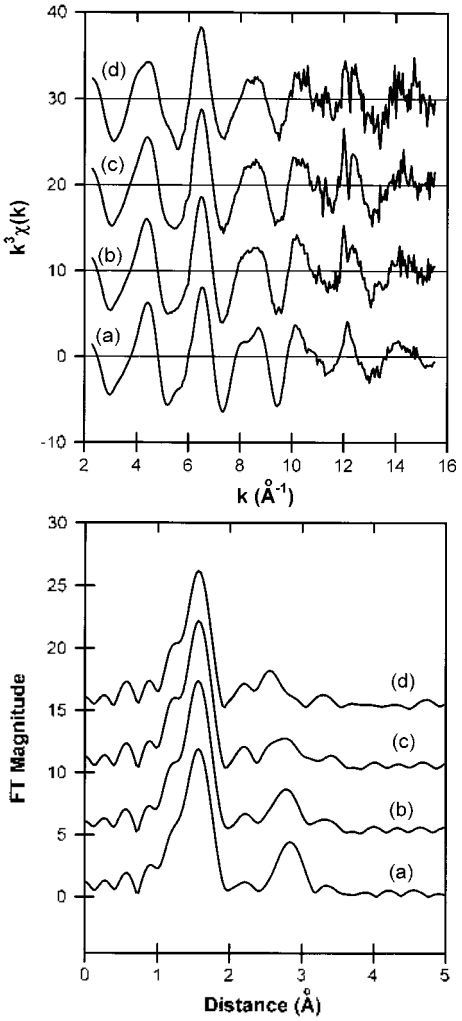

Figure 7. The k^3-weighted EXAFS spectra and their Fourier transforms for (a) TCF-Cl, (b) TCF-IM, (c) TCF-PILC250, and (d) TCF-PILC400.

The detailed information on crystal structure and bonding character was also obtained from EXAFS analysis. The k^3-weighted EXAFS oscillation was Fourier transformed in a k range of 2.5-13.5 $Å^{-1}$ as shown in Figure 7. According to the FT spectra (phase-shift uncorrected), the peak at ~2.9 Å, due to Cr-Cr pairs, disappears with an appearance of new ones at

Table 1. EXAFS Fitting Results for TCF-IM, TCF-PILCs and Reference Compounds Cr_2O_3

Compounds	Atom Pair	Distance (Å)	CN^a	σ^2 (10^{-3}Å^{-2})^b	E_0 shift (eV)^c
TCF-IM	$Cr\text{-}O_{ap}$	1.88	1	2.92	-1.00
	$Cr\text{-}O_{formate}$	1.97	4	3.50	-1.00
	$Cr\text{-}O_{H2O}$	2.02	1	3.00	-1.00
	Cr-C	2.94	8	5.55	-4.20
	Cr-Cr	3.29	2	8.01	-4.23
TCF-PILC250	$Cr\text{-}O_{ap}$	1.88	0.8	2.58	-0.10
	$Cr\text{-}O_{formate}$	1.97	4.0	3.21	-0.10
	$Cr\text{-}O_{H2O}$	2.01	1.0	3.51	-0.10
	Cr-C	2.99	4.5	5.56	0.88
	Cr-Cr	3.30	1.7	8.90	-5.23
TCF-PILC400	Cr-O	1.97	6.0	5.18	-2.39
	Cr-Cr	2.64	0.9	3.53	-9.23
	Cr-Cr	2.97	1.2	3.16	-6.26
	Cr-Cr	3.87	1.0	5.00	-4.52
Cr_2O_3	Cr-O	1.99	6.0	3.33	0.61
	$Cr\text{-}Cr_{face}$	2.66	1.0	5.73	-0.44
	$Cr\text{-}Cr_{edge}$	2.91	3.0	3.30	-0.44
	$Cr\text{-}Cr_{edge}$	3.42	3.0	3.04	-0.44
	$Cr\text{-}Cr_{corner}$	3.66	6.0	5.57	-0.44

[a]Coordination number. [b]Debye-Waller factor. [c]Threshold energy difference.

~2.3 Å and ~2.6 Å upon heating. The nonlinear least-squares curve fitting was carried out using the theoretical standard calculated from the structure of TCF-Cl.[25] The best fitting results for TCF-IM and TCF-PILC400 are summarized in Table 1 and Figure 8.

According to the EXAFS curve fitting result, the local structure around chromium in TCF-IM is identical with that in the standard salt, TCF-Cl, indicating that the basic structure of TCF ion itself is not altered by intercalation. In the case of TCF-PILC400, however, the Cr-Cr distance of vertex-linked CrO_6 octahedron (3.29 Å) in the precursor TCF ion splits into 2.64 Å, 2.97 Å, and 3.87 Å upon heating, corresponding to the face-, edge-, and corner-linked CrO_6 octahedra, respectively, similar to the local structure of chromium oxide, Cr_2O_3.[35] However, it is worthy to note here that the number of corner- and edge-shared neighbors decreases significantly compared to those of reference compound, Cr_2O_3, as shown in Table 1, implying that nano-sized chromia particles are stabilized in the interlayer space of clay, which is consistent with the basal spacing increment ($\Delta d \sim 6$ Å) in XRD.

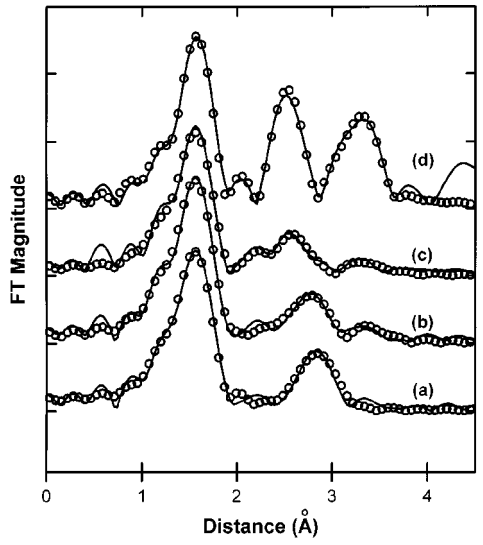

Figure 8. EXAFS fitting results for (a) TCF-Cl, (b) TCF-IM, (c) TCF-PILC400, and (d) Cr_2O_3.

Conclusion

In the present study, we prepare a chromia pillared clay by ion exchange reaction between Na^+ in montmorillonite with trimeric chromium oxyformate ions. Upon intercalation of TCF ion, the basal spacing of montmorillonite is expanded to 16.4 Å, suggesting that the Cr_3O plane is parallel to the aluminosilicate layers with a gallery height of ~6.8 Å. XANES, EPR, and diffuse reflectance spectroscopies confirm that the chromium ion is stabilized as Cr^{3+} in the interlayer space without any change of valency upon heat-treatment. EXAFS analyses reveal that the Cr-Cr distance of vertex-linkaged CrO_6 octahedron in the precursor TCF splits into three different distances during calcination corresponding to the face-, edge-, and corner-linkaged CrO_6 octahedra, respectively, similar to the local structure of the chromium oxide, Cr_2O_3. Therefore, it can be concluded that the TCF ion structure remains at 250 °C and transforms into nano-sized Cr_2O_3 particles in the interlayer space of montmorillonite at 400 °C, leading to the microporous pillared montmorillonite with the BET specific surface area of 152 m^2/g.

Acknowledgment. This study was supported by the Korea Ministry of Science and Technology through the National Research Laboratory Program '99, and in part by the Brain Korea 21 program. We thank Prof. M. Nomura for helping the synchrotron radiation experiments.

References

1. Han, Y.-S.; Yamanaka, S.; Choy, J.-H. *J. Solid State Chem.* **1999**, *144*, 45.
2. Pinnavaia, T. J. *Science* **1988**, *220*, 365.
3. Corma, A. *Chem. Rev.* **1997**, *97*, 2373.
4. Brindley, G. W.; Yamanaka, S. *Am. Mineral.* **1979**, *64*, 830.
5. Kundson, M. L.; McAtee, J. L. *Clay and Clay Miner.* **1973**, *21*, 19.
6. Brindley, G. W.; Sempels, R. E. *Clay Minerals* **1977**, *12*, 229.
7. Choy, J.-H.; Park, J.-H.; Yoon, J.-B. *J. Phys. Chem.* **1998**, *102*, 5991.
8. Burch, R. *Catalysis Today* **1988**, *2*, 1.
9. Pinnavaia, T. J.; Tzou, M. S.; Landau, S. D. *J. Am. Chem. Soc.* **1985**, *107*, 4783.
10. Kanai, H. *J. Catalysis* **1992**, *138*, 611.
11. Carr, R. M. *Clay and Clay Miner.* **1985**, *33*, 357.
12. Volzone, C. *Clays and Clay Miner.* **1995**, *43*, 377.
13. Pinnavaia, T. J.; Tzou, M.-S.; Landau, S. D.; Raythantha, R. H. *J. Mol. Catal.* **1984**, *27*, 195.

14. Mosset, A.; Galy, J. In *Synchrotron Radiation in Chemistry and Biology I*; Mandelkow, E., Ed.; Springer-Verlag: Berlin, 1988; pp 1-28.
15. Choy, J.-H.; Kim, D.-K.; Park, J.-C.; Choi, S.-N.; Kim, Y.-J. *Inorg. Chem.* **1997**, *36*, 189.
16. Choy, J.-H.; Yoon, J.-B.; Kim, D.-K.; Hwang, S.-H. *Inorg. Chem.* **1995**, *34*, 6524.
17. Choy, J.-H.; Park, J.-H.; Yoon, J.-B. *Photon Factory Activity Report* **1998**, *15*, 155.
18. Earnshaw, A.; Figgis, B. N. *J. Chem. Soc.(A)* **1966**, 1656.
19. Nomura, M.; Koyama, A.; Sakurai, M. *KEK Report* **1991**, 91-1.
20. Teo, B. K. *EXAFS: Basic Principles and Data Analysis*; Springer-Verlag: Berlin, 1986.
21. Sayers, D. E.; Bunker, B. A. In *X-ray Absorption: Principles, Applications, Techniques of EXAFS, SEXAFS, and XANES*; Koningsberger, D. C., Prins, R., Eds.; Wiley-Interscience: New York, 1988; pp 211-253
22. Newville, M.; Livins, P.; Yacoby, Y.; Rehr, J. J.; Stern, E. A. *Phys. Rev. B* **1993**, *47*, 14126.
23. Mustre de Leon, J.; Rehr, J. J.; Zabinsky, S. I. *Phys. Rev. B* **1991**, *44*, 4146.
24. O'Day, P. A.; Rehr, J. J.; Zabinsky, S. I.; Brown, Jr., G. E. *J. Am. Chem. Soc.* **1994**, *116*, 2938.
25. Chang, S. C.; Jeffrey, G. A. *Acta Crystallogr. B* **1970**, *26*, 673.
26. Johnson, M. K.; Powell, D. B.; Cannon, R. D. *Spectrochimica Acta* **1981**, *37A*, 995.
27. Al'tshuler, S. A.; Kozyrev, B. M. *Electron Paramagnetic Resonance in Compounds of Transition Elements*; John Wiley & Son: New York, 1974.
28. Dubicki, L.; Day, P. *Inorg. Chem.* **1972**, *11*, 1868.
29. Reddy, J. P. *Coord. Chem. Rev.* **1969**, *4*, 73.
30. Naidu, Y. N.; Rao, J. L.; Lakshman, S. V. J. *Spectrochimica Acta* **1992**, *48A*, 1029.
31. Taran, M. N.; Langer, K.; Platonov, A. N.; Indutny, V. V. *Phys. Chem. Minerals* **1994**, *21*, 360.
32. Bornholdt, K.; Corker, J. M.; Evans, J.; Rummey, J. M. *Inorg. Chem.* **1991**, *30*, 2.
33. Wechuysen, B. M.; Schoonheydt, R. A.; Jehng, J.-M.; Wachs, I. E.; Cho, S. J.; Ryoo, R.; Kijistra, S.; Poels, E. *J. Chem. Soc., Faraday Trans.* **1995**, *91*, 3245.
34. Lytle, F. W.; Greegor, R. B. *Phys. Rev. B* **1988**, *37*, 1550.
35. Newnham, R. E.; de Haan, Y. M. *Z. Krist.* **1962**, *117*, 235.